A Flexible Phase-Insensitive System for Broadband CW-Terahertz Spectroscopy and Imaging

M. Yahyapour, N. Vieweg, A. Roggenbuck, F. Rettich, O. Cojocari, and A. Deninger

***Abstract*—We present a compact, robust, and flexible continuous-wave (CW) terahertz system, ideally suited for both imaging and high-resolution broadband spectroscopy. The setup employs an incoherent detection scheme: A photomixer transmitter is combined with a zero-bias Schottky diode on the receiver side. The useable bandwidth extends to 1500 GHz, with a spectral resolution on the 10 MHz level. In proof-of-principle measurements, we apply our setup to imaging of objects within a paper envelope as well as transmission and reflection-mode spectroscopy, taking advantage of the high spectral resolution of the terahertz source and the broad bandwidth and efficiency of the Schottky receiver.**

***Index Terms*—Frequency-domain terahertz spectroscopy, incoherent detection, photomixer, terahertz imaging, zero-bias Schottky diode.**

I. Introduction

A PLURALITY of security [1] and nondestructive-testing applications [2] calls for terahertz instruments that both generate an image and perform a spectroscopic analysis of samples under test. Continuous-wave (CW) systems based on photomixing appear as promising candidates, owing to their broadband-tuning characteristics on one side and the flexibility in the choice of the frequency on the other side—the frequency employed for terahertz imaging can be selected according to the transmission properties and image resolution required. Indeed, photomixing systems have proven to be applicable in a broad range of applications, including spectroscopy of gases and solids [3], [4], imaging of medical samples [5], nondestructive testing of plastics [6], and astronomy [7].

The CW-terahertz generation process is based on heterodyne difference frequency generation in high-bandwidth photoconductors: The beat signal of two lasers is converted into a CW-terahertz wave, exactly at the difference frequency of the lasers. In comparison to time-domain terahertz systems, a CW-terahertz setup enables spectrally selective measurements, offers a significantly better frequency resolution, and has advantages both in terms of mechanical robustness and material costs. Over the past few years, CW-terahertz systems have matured considerably, and recently reached dynamic-range levels in excess of 100 dB and a spectral bandwidth greater than 3 THz [8]–[10].

Manuscript received April 18, 2016; accepted June 22, 2016. Date of publication August 12, 2016; date of current version August 31, 2016.

M. Yahyapour, N. Vieweg, A. Roggenbuck, F. Rettich, and A. Deninger are with TOPTICA Photonics AG, Munich 82166, Germany (e-mail: milad.yahyapour@toptica.com; nico.vieweg@toptica.com; axel.roggenbuck@toptica.com; florian.rettich@toptica.com; anselm.deninger@toptica.com).

O. Cojocari is with ACST GmbH, Hanau 63457, Germany (e-mail: oleg.cojocari@acst.de).

Color versions of one or more of the figures in this paper are available online at http://ieeexplore.ieee.org.

Digital Object Identifier 10.1109/TTHZ.2016.2589540

In a typical coherent-detection experiment, a first photomixer generates the CW-terahertz wave and a second photomixer serves as a terahertz receiver, producing a photocurrent signal that is sensitive to the *phase* of the incident terahertz wave. Data acquisition thus necessitates the use of either a delay-stage [11], [12] or highly accurate means for frequency control [13]. The phase data are exploited in spectroscopy, e.g., for refractive-index measurements [13], or for layer thickness assessments [14]. On the other hand, an inherent disadvantage of coherent-detection schemes is a rather limited flexibility to changes in the length of the terahertz beam path [12], [15], [16]. Furthermore, in imaging applications, the signal phase must be adjusted for each pixel individually, in order to compensate for variations in the thickness or material composition of the sample. In practice, therefore, a coherent-detection system is simply too slow for terahertz imaging.

Recently, Schottky detectors with a broadband response in the terahertz range [17] have become commercially available. The Schottky receiver works as "power law detector", producing a signal that has no phase relation with that of the transmitter-photomixer.

Schottky receivers have already been used successfully in conjunction with optoelectronic terahertz sources. Authors from TOPTICA Photonics AG and ACST GmbH have shown that a fast, AC-coupled Schottky receiver can measure the field intensity of individual terahertz pulses [18]. Ito *et al*. described a broadband polarization-sensitive Schottky receiver, which operated at frequencies from 30 GHz to 1 THz. However, the receiver still had a rather low sensitivity of approx. 300 V/W at 100 GHz and 4 V/W at 1000 GHz [19]. Han *et al*. demonstrated terahertz imaging with a line array of 20 zero-bias Schottky diodes, employing either a photoconductive switch or a CW-Gunn diode as terahertz sources. Yet, the 3 dB bandwidth of the receivers turned out to be limited to 180 GHz [20]. Nagatsuma *et al*. combined a uni-travelling-carrier photodiode with a Schottky receiver to build an optical-coherence tomography system. Whilst their system enabled precise thickness measurements, the reflection properties of the utilized beam splitter limited the useable frequency range to 400–800 GHz [21].

In this work, we combine a photomixer as a CW-terahertz source with a *broadband*, DC-coupled Schottky receiver, and we demonstrate the suitability of this incoherent assembly for both imaging and high-resolution terahertz spectroscopy. Our system accesses the entire frequency range from 50 to 1500 GHz with a frequency resolution on the 10 MHz level. It thus lends itself to terahertz imaging at any frequency within the aforementioned range, as well as for spectroscopic investigations, without the need for any beam-path realignments in between.

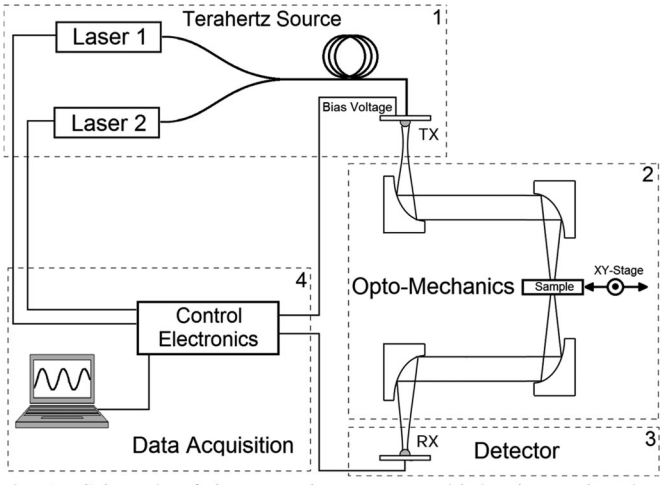

Fig. 1. Schematic of the CW-terahertz system with incoherent detection, aligned for transmission-mode measurements.

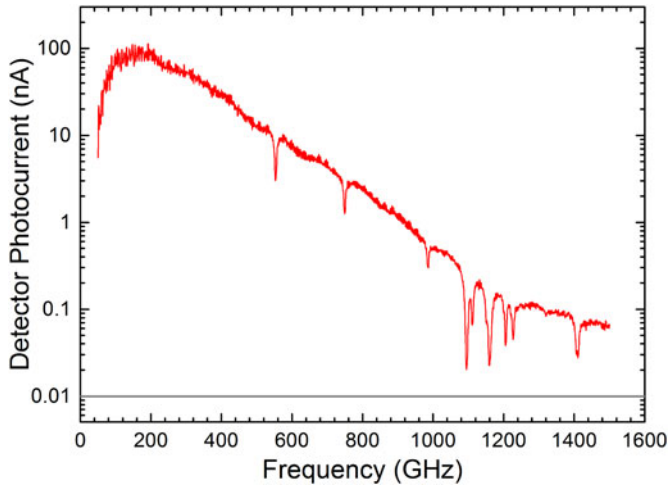

Fig. 2. Terahertz spectrum of air with water vapor absorption lines. The horizontal line at 10 pA indicates the noise floor.

II. Experimental Setup

Fig. 1 shows a schematic of our setup, the four main units being the following:

1) the terahertz source, which generates CW terahertz radiation;
2) an optomechanical assembly, which guides and shapes the terahertz beam, and creates a focus for imaging applications;
3) a detection unit, which measures the intensity of the incident terahertz wave;
4) control electronics and software for data acquisition.

In this work, we employed a GaAs photomixer with an integrated log-spiral antenna (model PM-Tx, Radiometer Physics GmbH). The device is illuminated by a pair of distributed feedback (DFB) diode lasers at center wavelengths of 783 and 785 nm (DL DFB, TOPTICA Photonics). The emission wavelengths are changed by heating or cooling the two laser diodes. The advantage of the system is its wide tuning range of $\sim$2 THz, which is achieved with only one pair of lasers [13]. A 3 dB coupler made of single-mode, polarization-maintaining fiber combines the two laser beams and guides the light to the terahertz transmitter. The optical power on the emitter chip is approx. 30 mW. The photomixer, described in detail elsewhere [11], [15], [22], emits a circularly polarized beam with a near-Gaussian beam pattern [23]. According to the manufacturer, the terahertz output amounts to approximately 1.4 μW at 100 GHz and 0.1 μW at 1000 GHz.

The optomechanical setup includes four off-axis parabolic mirrors with a focal length of 2 in. The sample is placed at the beam focus (spot size 2 mm). The optomechanics are mounted on rails, which can be conveniently rearranged for either transmission or reflection measurements. The sample is attached to an XY-scanning stage, which is raster-scanned through the beam focus in order to acquire an image.

The detector is a zero-bias Schottky diode (model 2DL 12C LS 1200 A1, ACST GmbH), likewise with an integrated log-spiral antenna. The useable bandwidth is 1.5 THz, and the responsivity ranges from 25 000 V/W at 100 GHz to about 2000 V/W at 1000 GHz. The noise equivalent power (NEP) is 7 $\mathrm{pW}/\sqrt{\mathrm{Hz}}$ at 100 GHz and 100 $\mathrm{pW}/\sqrt{\mathrm{Hz}}$ at 1000 GHz. The module includes a dc-coupled amplifier with an electric bandwidth of 1 MHz, which converts the current output of the Schottky diode to a voltage signal.

To tune the terahertz frequency, the electronics controls the wavelengths of the two DFB lasers with the help of a closed loop that acts on the chip temperatures, with a resolution of 40 μK [9]. The electronics also feeds an ac bias voltage (0/+11 V, 8 kHz) to the terahertz emitter. A digital lock-in amplifier [13] demodulates the receiver signal at the same frequency. A LabVIEW-based software program is used for data acquisition and subsequent analysis.

III. Results and Discussion

A. Spectroscopy

Fig. 2 depicts a spectrum of water vapor absorption lines in air. The frequency range of 50–1500 GHz was scanned in steps of 50 MHz. Across the spectrum, the detector output varies by almost four orders of magnitude, which underlines the high dynamic range of the receiver and the readout electronics. Towards higher frequencies, both the photomixer output and the detection efficiency of the Schottky diode decrease. Still, all of the prominent water lines at 557, 752, 988, 1098, 1113, 1163, 1208, 1229 and 1411 GHz are resolved [24]. The noise level is about 10 pA. We note that whilst the step size of 50 MHz already corresponds to a temperature increment of 1 mK per laser, this is not yet the limit: with the same control electronics, we demonstrated frequency steps as small as 1 MHz [9].

It is instructive to compare the frequency-dependent responsivity of the photomixer and the detector. In the spectrum shown in Fig. 2, the receiver signal drops by a factor of $\sim$150 between 100 and 1000 GHz. Assuming that the photomixer efficiency accounts for a factor of 14 (the ratio of the power values as stated above), the responsivity of the Schottky receiver decreases by a

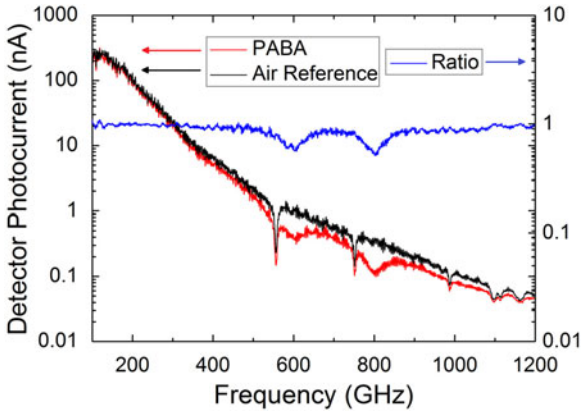

Fig. 3. Terahertz spectrum of PABA (red trace) and an air reference (black trace, left scale). The blue trace shows the normalized ratio spectrum (right scale).

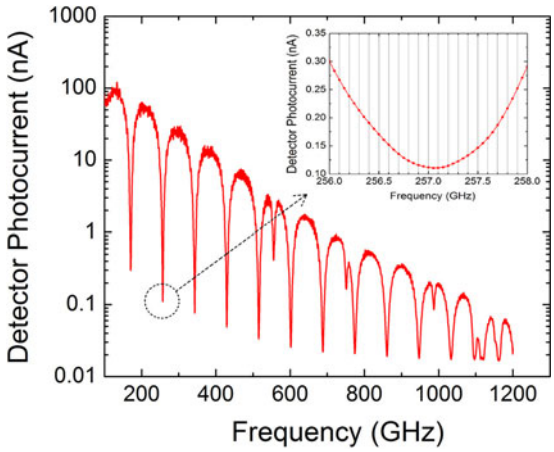

Fig. 4. Reflection spectrum of a silicon wafer measured with 50 MHz spectral resolution (see inset).

factor of 11. This is in good agreement with the ratio of the specified responsivity values (25 000 V/W : [2000 V/W] = 12.5).

Fig. 3 shows a transmission spectrum of a 1.8-mm-thick sample of 4-aminobenzoic acid (PABA, red curve), an air reference (black curve) and the ratio of both spectra (blue curve). In the normalized spectrum, the water lines at 557 and 752 GHz are no longer seen. Instead, the normalization reveals the PABA absorption lines at 600 and 800 GHz along with their FWHM linewidths of 70 and 55 GHz, respectively. The values are in excellent agreement with time-domain terahertz measurements published by Palka [25].

Fig. 4 depicts a reflection spectrum of a silicon wafer. The wafer acts as a Fabry–Pérot etalon, producing a sequence of pronounced, equidistant dips in the spectrum. Note that the reflection minima above 900 GHz, as well as the water lines at 1098 and 1163 GHz, appear somewhat broadened as they approach the noise level of this measurement.

Using the well-known relation between the free spectral range FSR, the sample thickness d, refractive index n, refraction angle θ and the vacuum speed of light c_0

$$\mathrm{FSR} = \frac{c_0}{2dn\cos\theta}$$

Fig. 5. Terahertz transmission image of an envelope containing a PCB, a key, a pair of scissors, and a paperclip. The color bar represents a linear intensity scale in arbitrary units. The minimum intensity value is 0 and the maximum value is 120. Except for the choice of the color scale, no postprocessing or averaging was applied.

we employ the spectrum of Fig. 4 to determine the thickness of the silicon sample. The refraction angle $\theta = 12° \pm 0.2°$ is obtained from Snell's law, considering an incident angle of 45° $\pm$ 1°. The refractive index of high-resistivity silicon is 3.376 $\pm$ 0.004 [11]. From the spectrum, we infer FSR $\cong$ 86.3 $\pm$ 0.2 GHz. We thus obtain a sample thickness of 526 $\pm$1 μm, which agrees within 0.2% with the value of 525 μm as measured with a micrometer screw.

B. Imaging

Fig. 5 shows a terahertz transmission image of a paper envelope of 135 mm length and 52 mm width, which contained a pair of scissors, a key, a printed circuit board (PCB), and a paper clip. The envelope was mounted on an XY translation stage. The emitter frequency was fixed at 450 GHz. The field of view was 450 $\times$ 173 pixels, with a pixel size of 0.3 $\times$ 0.3 mm^2. The lock-in integration time was 300 ms per pixel.

In the image, the color bar represents a linear intensity scale. Red and blue sections correspond to maximum and minimum signal levels, respectively. The wire of the paper clip has a diameter of 1 mm and is still clearly resolved. The holes in the PCB, 2 mm and 3 mm in diameter, are also seen, as are the conducting paths (width 1 mm). Note that the epoxy substrate of the PCB appears "semitransparent" at 450 GHz.

The spatial resolution of the image is approx. 1 mm, which is roughly the size of the wavelength (0.66 mm). Sharper focussing and/or a higher working frequency could improve the resolution further.

The acquisition time of a CW-terahertz image generally depends on the speed of the translation stage, the pixel size, and the lock-in integration time per pixel. Our proof-of-principle image was recorded during an overnight measurement, the stop-and-measure movement of the translation stage being the "speed limit". With a faster, continuously moving translation stage, shorter integration times (e.g., 1 ms instead of 300 ms) and a reduced pixel size (e.g., 1 mm), we envisage an image acquisition time on the order of 10 s.

Commercially available terahertz cameras based on high-electron-mobility transistor (HEMT) arrays still achieve significantly higher frame rates [26]. On the other hand, the NEP of a multipixel camera is typically on the order of 1 nW/$\sqrt{\mathrm{Hz}}$, which is $\sim$140 times less sensitive than the Schottky receiver described here. In conjunction with

optoelectronic sources, HEMTs thus only work for frequency up to 700 GHz [26]. The bandwidth of the Schottky receiver is two times higher, which underlines the suitability of our system for wide-band "spectroscopic imaging."

IV. Conclusion

We have presented a broadband CW terahertz system with a photoconductive transmitter and a zero-bias Schottky detector. The bandwidth of 1500 GHz is more than two times larger than that of multi-pixel cameras, and three times larger than that of previous systems of similar design [21]. Indeed, the bandwidth is comparable to that of a coherent, photomixing system, yet in contrast to coherent detection schemes, our setup not only offers a greater flexibility with respect to the length of the terahertz beam path, but also speeds up the acquisition time for transmission or reflection spectra. Both applications were demonstrated in "proof-of-principle" measurements.

The phase-insensitive detection scheme facilitates terahertz imaging, too. In contrast to coherent-detection systems, which call for a well-controlled (and time-consuming) phase modulation at each image pixel, the setup presented here accomplishes a single-pixel intensity measurement within less than a millisecond. We envisage that the system can be used for real-time monitoring of foreign bodies in plastics, nappies, or cardboard boxes. If a fixed-frequency inspection reveals the presence of a suspicious object, additional spectral information can be gained—without shifting the sample or the measurement setup.

Acknowledgment

The authors would like to thank A. Moreau for excellent experimental support and K. Dutzi for careful proofreading of the manuscript.

References

[1] H. Liu *et al.*, "Terahertz spectroscopy and imaging for defense and security applications," *Proc. IEEE*, vol. 95, no. 8, pp. 1514–1527, Aug. 2007.
[2] K. Kawase *et al.*, "Non-destructive terahertz imaging of illicit drugs using spectral fingerprints," *Opt. Exp.*, vol. 11, no. 20, pp. 2549–2554, 2003.
[3] P. U. Jepsen, D. G. Cooke, and M. Koch, "Terahertz spectroscopy and imaging - Modern techniques and applications," *Laser Photon. Rev.*, vol. 5, no. 1, pp. 124–166, 2011.
[4] D. Saeedkia (Ed.), *Handbook of Terahertz Technology for Imaging, Sensing, and Communications*, ser. Electron. Opt. Mater., no 34, Sawston, Cambridge, U.K.: Woodhead Publishing, 2013.
[5] K. J. Siebert *et al.*, "Continuous-wave all-optoelectronic terahertz imaging," *Appl. Phys. Lett.*, vol. 80, no. 16, pp. 3003–3005, 2002.
[6] M. Scheller *et al.*, "Terahertz quasi-time-domain spectroscopy imaging.," *Appl. Opt.*, vol. 50, no. 13, pp. 1884–1888, 2011.
[7] I. Cámara Mayorga *et al.*, "First in-field application of a full photonic local oscillator to terahertz astronomy," *IEEE Trans. Terahertz Sci. Technol.*, vol. 2, no. 4, pp. 393–399, Jul. 2012.
[8] T. Göbel *et al.*, "Telecom technology based continuous wave terahertz photomixing system with 105 decibel signal-to-noise ratio and 3.5 terahertz bandwidth," *Opt. Lett.*, vol. 38, no. 20, pp. 4197–9, 2013.
[9] A. Deninger *et al.*, "2.75 THz tuning with a triple-DFB laser system at 1550 nm and InGaAs photomixers," *J. Infrared Millim. Terahertz Waves*, vol. 36, no. 3, pp. 269–277, 2015.
[10] J. Kim *et al.*, "CW-THz vector spectroscopy and imaging system based on 1.55-μm fiber-optics," *Opt. Exp.*, vol. 22, no. 2, pp. 1735–1741, 2014.
[11] A. Roggenbuck *et al.*, "Using a fiber stretcher as a fast phase modulator in a continuous wave terahertz spectrometer," *J. Opt. Soc. Amer. B*, vol. 29, no. 4, pp. 614–620, 2012.
[12] T. Probst, A. Rehn, and M. Koch, "Compact and low-cost THz QTDS system," *Opt. Exp.*, vol. 23, no. 17, pp. 21972–21982, 2015.
[13] A. Roggenbuck *et al.*, "Coherent broadband continuous-wave terahertz spectroscopy on solid-state samples," *New J. Phys.*, vol. 12, no. 4, pp. 043017–043029, 2010.
[14] D. Stanze *et al.*, "Multilayer thickness determination using continuous wave THz spectroscopy," *IEEE Trans. THz Sci. Technol.*, vol. 4, no. 6, pp. 696–701, Nov. 2014.
[15] M. Langenbach *et al.*, "Group delay in THz spectroscopy with ultra-wideband log-spiral antennae," *J. Infrared Millim. Terahertz Waves*, vol. 35, pp. 918–931, 2014.
[16] W.-G. Yeo and N. K. Nahar, "Characterization of a THz CW spectrometer pumped at 1550 nm," *Infrared Phys. Technol.*, vol. 71, pp. 70–76, 2015.
[17] A. Semenov *et al.*, "Application of zero-bias quasi-optical schottky-diode detectors for monitoring short-pulse and weak terahertz radiation," *IEEE Electron Device Lett.*, vol. 31, no. 7, pp. 674–676, Jul. 2010.
[18] F. Rettich *et al.*, "Field intensity detection of individual terahertz pulses at 80 MHz repetition rate," *J. Infrared Millim. Terahertz Waves*, vol. 36, no. 7, pp. 607–612, 2015.
[19] H. Ito *et al.*, "Polarisation-sensitive sub-terahertz-wave detector implementing antenna-integrated zero-bias Schottky barrier diode," *Electron. Lett.*, vol. 49, no. 15, pp. 949–950, 2013.
[20] S.-P. Han *et al.*, "InGaAs Schottky barrier diode array detector for a real-time compact terahertz line scanner," *Opt. Exp.*, vol. 21, no. 22, pp. 25874–25882, 2013.
[21] T. Nagatsuma, H. Nishii, and T. Ikeo, "Terahertz imaging based on optical coherence tomography," *Photon. Res.*, vol. 2, no. 4, pp. B64–B69, 2014.
[22] I. Cámara Mayorga *et al.*, "Terahertz photomixing in high energy oxygen- and nitrogen-ion-implanted GaAs," *Appl. Phys. Lett.*, vol. 91, no. 3, 2007, Art. no. 031107.
[23] M. Nagel *et al.*, "Continuous-wave terahertz near-field spectroscopy and imaging with a micro-machined photomixer probe-tip," in *Proc. 37th Int. Conf. Infrared, Millimeter Terahertz Waves*, 2012.
[24] L. S. Rothman *et al.*, "The HITRAN 2012 molecular spectroscopic database," *JQSRT*, vol. 130, pp. 4–50, 2013.
[25] N. Palka, "THz Reflection spectroscopy of explosives measured by time domain spectroscopy," *Acta Phys. Pol. A*, vol. 120, no. 4, pp. 713–715, 2011.
[26] "Terasense Terahertz Imaging Cameras." [Online]. Available: http://terasense.com/products/sub-thz-imaging-cameras/. [Accessed on: Apr. 12, 2016].

M. Yahyapour, photograph and biography not available at the time of publication.

N. Vieweg, photograph and biography not available at the time of publication.

A. Roggenbuck, photograph and biography not available at the time of publication.

F. Rettich, photograph and biography not available at the time of publication.

O. Cojocari, photograph and biography not available at the time of publication.

A. Deninger, photograph and biography not available at the time of publication.